Chapter 2
Wind Regimes

The principal origin of the winds in the Earth's atmosphere and the potentially available power from these winds have been qualitatively described in Sect. 1.4. This general description of the driving forces for the wind has to be brought into a mathematical formulation for precise turbine load and energy yield calculations and predictions. Therefore, this chapter will present the basic wind laws in the free atmosphere and will introduce the basic features of atmospheric thermal stability. Vertical wind profiles in atmospheric boundary layers over different surface types will be presented in the subsequent Chaps. 3–5.

2.1 Global Circulation

Flow patterns and winds emerge from horizontal surface and atmospheric temperature contrasts on all spatial scales from global to local size. Globally, the tropical belt and the lower latitudes of the Earth are the main input region for solar energy, while the higher latitudes and the poles are the regions with a negative energy balance, i.e. the Earth here loses energy through thermal radiation. Ocean currents and atmospheric heat conduction are not sufficient to compensate for this differential heating of the globe. The global atmospheric circulation has to take over as well. Main features of this global atmospheric circulation are the Hadley cell, the Ferrel cell and the polar cell which become visible from a latitude-height plot showing an average overall longitudes of the winds in the troposphere and stratosphere. The Hadley cell exhibits a direct thermal circulation. Warm air rises near the equator, moves towards the poles aloft and descends in the subtropics. The region of sinking motion is characterized by large anticyclones in the surface pressure field and deserts. Likewise, the polar cell exhibits a direct thermal circulation as well. Here, cold air sinks over the poles and rises at higher latitudes. This is the reason for generally high pressure over the poles. In between the Hadley cell and the polar cell lies the thermally indirect Ferrel cell. This cell is characterized by

S. Emeis, *Wind Energy Meteorology*, Green Energy and Technology,
https://doi.org/10.1007/978-3-319-72859-9_2

rising colder air at higher latitudes and sinking warmer air in the subtropics. This circulation is indirect and it is the result of the integral effect overall the moving cyclones in this belt of temperate latitudes. Effectively, the Ferrel cells transports warmer air towards the poles near the ground and colder air towards the tropics aloft. This indirect circulation is maintained by energy conversions from potential energy into kinetic energy in the moving cyclones of the temperate latitudes.

The just described system of cells would only produce meridional winds, i.e. winds from south to north or vice versa. The Earth's rotation is modifying this meridional circulation system by the Coriolis force. Winds towards the poles get a westerly component, winds towards the equator an easterly component. Therefore, we mainly observe westerly winds at the ground in the Ferrel cell while we observe easterly winds at the ground in the Hadley cell and the polar cell. The northeasterly winds near the ground of the Hadley cell are also known as the trade winds. These global wind cells have a spatial scale of roughly 10,000 km. The global wind system is modified by the temperature contrasts between the continents and the surrounding oceans and by large north–south orientated mountain ranges, in particular those at the west coasts of the Americas. These modifications have a spatial scale of some 1000 km. Even smaller land–sea wind systems in coastal areas may have an order of 100 km; mountain and valley wind systems can be even smaller in the order of several tens of kilometres. All these wind systems may be suitable for wind power generation.

While the trade winds and the winds in the polar cell exhibit quite some regularity and mainly have seasonal variations, the winds in the Ferrel cell are much more variable in space and time. Near-surface wind speeds in normal cyclones can vary between calms and about 25 m/s within a few hours. Wind speeds in strong hibernal storms of the temperate latitudes can reach about 35–40 m/s while wind speeds in subtropical hurricanes easily reach more than 50 m/s. Cut-off wind speeds of modern wind energy turbines are between 25 and 30 m/s. Thus, strong storms in temperate latitudes may lead to phases where the wind potential can no longer be used. These hibernal storms are most likely in Northwestern Europe, Northeastern Canada, the Pacific coasts of Canada and Alaska as well as the southern tips of South America, Africa and Australia.

Hurricanes are called typhoons in Southeast Asia and cyclones in India. The occurrence of hurricanes can even threaten the stability of the construction of the turbines, because they can come with wind speeds above those listed in the IEC design standards. The hurricane risks have been investigated by Rose et al. (2012). In particular, the planning of offshore wind parks in hurricane-threatened areas needs special attention. According to the map of natural hazards published by the reinsurance company Munich Re, hurricane-prone areas are the southern parts of the Pacific coasts and the Atlantic coasts of the United States and Central America, Eastern India and Southeast Asia, Madagascar and the northern half of Australia.

There are very strong winds on even smaller scales such as thunderstorm downbursts, whirlwinds and tornados, but their variability and destructive force is

not suited for wind power generation. Rather turbines have to be constructed in a way that they can stand these destructive forces while being shut off. See also Sects. 2.6 and 6.5 for wind hazards.

2.2 Driving Forces

The equations in the following subchapters describe the origin and the magnitude of horizontal winds in the atmosphere. We will start with the full set of basic equations in Sects. 2.2.1 and 2.2.2 and will then introduce the usual simplifications which lead to the description of geostrophic and gradient winds in Sect. 2.3. Geostrophic and gradient winds, which blow in the free atmosphere above the atmospheric boundary layer, have to be considered as the relevant external driving force in any wind potential assessment and any load assessment. Vertical variations in the geostrophic and gradient winds are described by the thermal winds introduced in Sect. 2.4.

2.2.1 Hydrostatic Equation

The most basic explanation of the wind involves horizontal heat gradients. The sun heats the Earth's surface differently according to latitude, season and surface properties. This heat is transported upward from the surface into the atmosphere mainly by turbulent sensible and latent heat fluxes. This leads to horizontal temperature gradients in the atmosphere. The density of air, and with this density the vertical distance between two given levels of constant pressure, depends on air temperature. A warmer air mass is less dense and has a larger vertical distance between two given pressure surfaces than a colder air mass. Air pressure is closely related to air density. Air pressure is a measure for the air mass above a given location. Air pressure decreases with height. In the absence of strong vertical accelerations, the following hydrostatic equation describes this decrease:

$$\frac{\partial p}{\partial z} = -g\rho = -\frac{gp}{RT} \tag{2.1}$$

where p is air pressure, z is the vertical coordinate, g is the Earth's gravity, ρ is air density, R is the specific gas constant of air and T is absolute air temperature. With typical near-surface conditions (T = 293 K, R = 287 J kg^{-1} K^{-1}, p = 1000 hPa and g = 9.81 ms^{-2}), air pressure decreases vertically by 1 hPa each 8.6 m. In wintry conditions, when T = 263 K, pressure decreases 1 hPa each 7.7 m near the surface. At greater heights, this decrease is smaller because air density is decreasing with height as well. At a height of 5.5 km the air pressure is at about half of the surface value, and thus, the pressure only decreases by 1 hPa every 15 m. An (unrealistic) atmosphere at constant near-surface density would only be 8 km high!

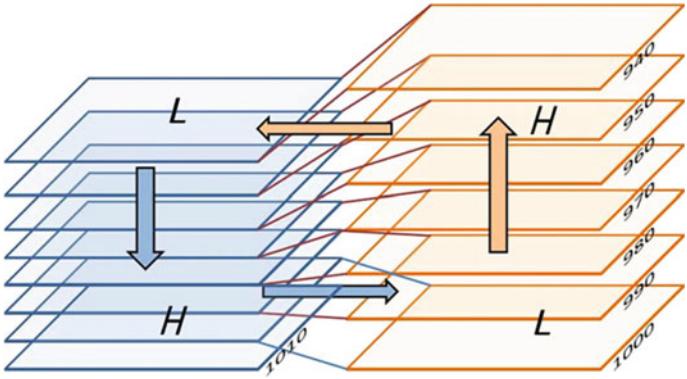

Fig. 2.1 Vertical pressure gradients in warmer (right) and colder (left) air. Planes symbolize constant pressure levels. Numbers give air pressure in hPa. Capital letters indicate high (H) and low (L) pressure at the surface (lower letters) and on constant height surfaces aloft (upper letters). Arrows indicate a thermally direct circulation

The consequence of (2.1) is that the pressure in warm air masses decreases more slowly with height than in cold air masses. Assuming a constant surface pressure, this would result in horizontal pressure gradients aloft. A difference in 30° in air mass temperature will cause a 1.36 hPa pressure gradient between the warm and the cold air mass 100 m above ground. This pressure gradient produces compensating winds which tend to remove these gradients. In reality, surface pressure sinks in the warmer region ('heat low'). This situation is depicted in Fig. 2.1. In a situation with no other acting forces (especially no Coriolis forces due to the rotating Earth), this leads to winds blowing from higher towards lower pressure. Such purely pressure-driven winds are found in land–sea and mountain–valley wind systems. This basic effect is depicted in term III in the momentum budget equations that will be introduced in the following subchapter.

2.2.2 Momentum Budget Equations for the Wind

A mathematical description of the winds is most easily done by considering the momentum balance of the atmosphere. Momentum is mass times velocity. The momentum budget equations are a set of differential equations describing the acceleration of the three wind components. In complete mass-specific form, they read (mass-specific means that these equations are formulated per unit mass, the mass-specific momentum has the physical dimension of a velocity. Therefore, we say wind instead of momentum in the following):

$$\frac{\partial u}{\partial t} + \vec{v}\nabla u + \frac{1}{\rho}\frac{\partial p}{\partial x} \qquad - fv + f^* w \qquad \mp v\frac{|\vec{v}|}{r} \qquad + F_x = 0 \qquad (2.2)$$

$$\frac{\partial v}{\partial t} + \vec{v}\nabla v + \frac{1}{\rho}\frac{\partial p}{\partial y} \qquad + fu \qquad \pm u\frac{|\vec{v}|}{r} \qquad + F_y = 0 \qquad (2.3)$$

$$\frac{\partial w}{\partial t} + \vec{v}\nabla w + \frac{1}{\rho}\frac{\partial p}{\partial z} \qquad - g \qquad - f^* u \qquad + F_z = 0 \qquad (2.4)$$

I II III IV V VI VII

where u is the wind component blowing into positive x direction (positive in eastward direction), v is the component into y direction (positive in northward direction) and w is the vertical wind (positive upward). The wind vector is $\vec{v} = (u, v, w)$, the horizontal Coriolis parameter is $f = 2\Omega \sin\varphi$ where Ω is the rotational speed of the Earth and φ is the latitude (see Table 2.1), the vertical Coriolis parameter is $f^* = 2\Omega \cos\varphi$, r is the radius of curvature, and F_x, F_y and F_z are the three components of the frictional forces, which will be specified later. Equations (2.2)–(2.4), which are called Eulerian equations of motion in meteorology, are a special form of the Navier–Stokes equations in hydrodynamics.

Term I in Eqs. (2.2)–(2.4) is called inertial or storage term, it describes the temporal variation of the wind components. The nonlinear term II expresses the interaction between the three wind components. Term III specifies the above-mentioned pressure force. Term IV, which is present in (2.4) only, gives the influence of the Earth's gravitation. Term V denotes the Coriolis force due to the rotating Earth. Term VI describes the centrifugal force in non-straight movements around pressure maxima and minima (the upper sign is valid for flows around lows, the lower sign for flows around high-pressure systems). The last term VII symbolizes the frictional forces due to the turbulent viscosity of air and surface friction.

Table 2.1 Latitude-dependent Coriolis parameter f in s^{-1} for the northern hemisphere

Latitude (in degrees)	Coriolis parameter in s^{-1}
30	0.727×10^{-4}
40	0.935×10^{-4}
50	1.114×10^{-4}
60	1.260×10^{-4}

The values in both columns are negative for the southern hemisphere

The terms in (2.2)–(2.4) may have different magnitudes in different weather situations and a scale analysis for a given type of motion may lead to discarding some of them. Nearly always, the terms containing f^* are discarded because they are very small compared to all other terms in the same equation. In larger scale motions, term VI is always neglected as well. Term VI is only important in whirl winds and close to the centre of high- and low-pressure systems. Looking at the vertical acceleration only [Eq. (2.4)], terms III and IV are dominating. Equating these two terms in (2.4) leads to the hydrostatic Eq. (2.1) above.

There is only one driving force in Eqs. (2.2)–(2.4): the above-mentioned pressure force which is expressed by term III. The constant outer force due to the gravity of the Earth (term IV) prevents the atmosphere from escaping into space. The only braking force is the frictional force in term VII. The other terms (II, V, and VI) just redistribute the momentum between the three different wind components. Thus, sometimes terms V and VI are named 'apparent forces'. In the special case when all terms II to VII would disappear simultaneously or would cancel each other perfectly, the air would move inertially at constant speed. This is the reason why term I is often called inertial term.

2.3 Geostrophic Winds and Gradient Winds

The easiest and most fundamental balance of forces is found in the free troposphere above the atmospheric boundary layer, because frictional forces are negligible there. Therefore, our analysis is started here for large-scale winds in the free troposphere. The frictional forces in term VII in Eqs. (2.2)–(2.4) can be neglected above the atmospheric boundary layer. The isobar curvature term VI is also very small and negligible away from pressure maxima and minima. The same applies to term II for large-scale motions with small horizontal gradients in the wind field. A scale analysis shows that the equilibrium of pressure and Coriolis forces is then the dominating feature when the situation is stationary and the inertial term I can be neglected as well. This leads to the following two equations:

$$-\rho f u_g = \frac{\partial p}{\partial y} \tag{2.5}$$

$$\rho f v_g = \frac{\partial p}{\partial x} \tag{2.6}$$

with u_g and v_g being the components of this equilibrium wind, which is usually called geostrophic wind in meteorology. The geostrophic wind is solely determined by the large-scale horizontal pressure gradient and the latitude-dependent Coriolis parameter, the latter being in the order of 0.0001 s^{-1} (see Table 2.1 for some

sample values). Because term VII had been neglected in the definition of the geostrophic wind, surface friction and the atmospheric stability of the atmospheric boundary layer have no influence on the magnitude and direction of the geostrophic wind. The modulus of the geostrophic wind reads:

$$\left|v_g\right| = \sqrt{u_g^2 + v_g^2} \tag{2.7}$$

The geostrophic wind blows parallel to the isobars of the pressure field on constant height surfaces. Following Eqs. (2.5) and (2.6), a horizontal pressure gradient of about 1 hPa per 1000 km leads to a geostrophic wind speed of about 1 m/s. In the northern hemisphere, the geostrophic wind blows counterclockwise around low-pressure systems and clockwise around high-pressure systems. In the southern hemisphere, the sense of rotation is opposite.

Term VI in Eqs. (2.2)–(2.4) is not negligible in case of considerably curved isobars. The equilibrium wind is the so-called gradient wind (Dutton 1986; Kristensen and Jensen 1999) in this case:

$$-\rho f u = \frac{\partial p}{\partial y} \pm \frac{\rho u \left|\overrightarrow{v}\right|}{r} \tag{2.8}$$

$$\rho f v = \frac{\partial p}{\partial x} \mp \frac{\rho v \left|\overrightarrow{v}\right|}{r} \tag{2.9}$$

Once again, the upper sign is valid for flows around lows, the lower sign for flows around high-pressure systems. The gradient wind around low-pressure systems is a bit lower than the geostrophic wind (because centrifugal force and pressure gradient force are opposite to each other), while the gradient wind around high-pressure systems is a bit higher than the geostrophic wind (here centrifugal force and pressure gradient force are unidirectional).

Sometimes, in rare occasions, the curvature of the isobars can be so strong that the centrifugal force in term VI is much larger than the Coriolis force in term V so that an equilibrium wind forms which is governed by pressure forces and centrifugal forces only. This wind, called cyclostrophic wind by meteorologists, is found in whirl winds and tornados.

The geostrophic wind and the gradient wind are not height-independent in reality. Horizontal temperature gradients on levels of constant pressure lead to vertical gradients in these winds. The wind difference between the geostrophic winds or gradient winds at two different heights is called the thermal wind (see Sect. 2.4). Only in the absence of thermal winds, the surface pressure gradients can be used to determine the geostrophic winds aloft.

2.4 Thermal Winds

We introduced in Sect. 2.3 the geostrophic wind as the simplest choice for the governing large-scale forcing of the near-surface wind field. The geostrophic wind is an idealized wind which originates from the equilibrium between pressure gradient force and Coriolis force. Until now we have always anticipated a barotropic atmosphere within which the geostrophic wind is independent of height, because we assumed that the horizontal pressure gradients in term III of (2.2) and (2.3) are independent of height. This is not necessarily true in reality and the deviation from a height-independent geostrophic wind can give an additional contribution to the vertical wind profile as well. The horizontal pressure gradient becomes height-dependent in an atmosphere with a large-scale horizontal temperature gradient. Such an atmosphere is called baroclinic and the difference in the wind vector between geostrophic winds at two heights is called thermal wind. The real atmosphere is nearly always at least slightly baroclinic, thus the thermal wind is a general phenomenon.

Thermal winds do not depend on surface properties. So they can appear over all surface types addressed in Chaps. 3–5.

Differentiation of the hydrostatic Eq. (2.1) with respect to y and differentiation of the definition equation for the u-component of the geostrophic wind (2.5) with respect to z leads after the introduction of a vertically averaged temperature T_M to the following relation for the height change of the west–east wind component u:

$$\frac{\partial u}{\partial z} = -\frac{g}{fT_M}\frac{\partial T_M}{\partial y} \tag{2.10}$$

Subsequent integration over the vertical coordinate from the roughness length z_0 to a height z gives finally for the west–east wind component at the height z:

$$u(z) = u(z_0) - \frac{g(z - z_0)}{fT_M}\frac{\partial T_M}{\partial y} \tag{2.11}$$

The difference between $u(z)$ and $u(z_0)$ is the u-component of the thermal wind. A similar equation can be derived for the south–north wind component v from Eqs. (2.1) and (2.6):

$$v(z) = v(z_0) + \frac{g(z - z_0)}{fT_M}\frac{\partial T_M}{\partial x} \tag{2.12}$$

Following (2.10) and (2.11), the increase of the west–east wind component with height is proportional to the south–north decrease of the vertically averaged temperature in the layer between z_0 and z. Likewise, (2.12) tells us that the south–north wind component increases with height under the influence of a west–east temperature increase. Usually, we have falling temperatures when travelling north in the

west wind belt of the temperate latitudes on the northern hemisphere, so we usually have a vertically increasing west wind on the northern hemisphere.

Equations (2.11) and (2.12) allow for an estimation of the magnitude of the vertical shear of the geostrophic wind, i.e. the thermal wind from the large-scale horizontal temperature gradient. The constant factor $g/(fT_M)$ is about 350 m/(s K). Therefore, a quite realistic south–north temperature gradient of 10^{-5} K/m (i.e., 10 K per 1000 km) leads to a non-negligible vertical increase of the west–east wind component of 0.35 m/s per 100 m height difference.

The thermal wind also gives the explanation for the vertically turning winds during episodes of cold air or warm air advection. Imagine a west wind blowing from a colder to a warmer region. Equation (2.12) then gives an increase in the south–north wind component with height in this situation. This leads to a backing of the wind with height. In the opposite case of warm air advection, the wind veers with height.

2.5 Boundary Layer Winds

The wind speed in the atmospheric boundary layer must decrease to zero towards the surface due to the surface friction (no-slip condition). The atmospheric boundary layer can principally be divided into three layers in the vertical. The lowest layer which is only a few millimetres deep is laminar and of no relevance for wind energy applications. Then follows the surface layer (also called constant flux layer or Prandtl layer), which may be up to about 100 m deep, where the forces due to the turbulent viscosity of the air dominate, and within which the wind speed increases strongly with height. The third and upper layer, which usually covers 90% of the boundary layer, is the Ekman layer. Here, the rotational Coriolis force is important and causes a turning of the wind direction with height. The depth of the boundary layer varies between about 100 m at night with low winds and about 2–3 km at daytime with strong solar irradiance.

Scale analysis of the momentum Eqs. (2.2)–(2.4) for the boundary layer shows the dominance of terms III, V and VII. Sometimes, for low winds in small-scale motions and near the equator, the pressure force (term III) is the only force and a so-called Euler wind develops, which blows from higher pressure towards lower pressure. Such nearly frictionless flows rarely appear in reality. Usually, an equilibrium between the pressure force and the frictional forces (terms III and VII) is observed in the Prandtl layer, and an equilibrium between the pressure force, the Coriolis force and the frictional forces (terms III, V, and VII) is observed in the Ekman layer. The Prandtl layer wind is sometimes called antitriptic wind. No equation for the antitriptic winds analog to (2.5), (2.6) or (2.8), (2.9) is available, since neither term III nor term VII contains explicitly the wind speed.

The Prandtl layer is characterized by vertical wind gradients. The discussion of Prandtl layer wind laws which describe these vertical wind speed gradients is postponed to Chap. 3. The vertical gradients are much smaller in the Ekman layer,

so that it is meaningful to look at two special cases of (2.2) and (2.3) in the following subchapter.

In a stationary Ekman layer the terms III, V and VII balance each other, because term I vanishes. This layer is named from the Swedish physicist and oceanographer W. Ekman (1874–1954), who for the first time derived mathematically the influence of the Earth's rotation on marine and atmospheric flows. A prominent wind feature in the Ekman layer is the turning of wind direction with height.

The vertical profiles of these boundary layer winds over different surface types will be analysed in more detail in the upcoming Chaps. 3–5.

2.6 Thunderstorm Gusts and Tornados

There are strong winds which cannot be used for wind energy generation, because they are short-lived and rare in time and place, such that their occurrence is nearly unpredictable. Most prominent among these phenomena are thunderstorm gusts and tornadoes. Offshore tornadoes are called waterspouts. They can be so violent that they can damage wind turbines. Therefore, the probability of their occurrence and their possible strength should be nevertheless investigated during the procedure of wind turbine siting.

2.6.1 Thunderstorm Gusts

Wind gusts linked to onshore thunderstorms have their maximum in the late afternoon, because onshore thunderstorms are most frequent in the afternoon and early evening. Gusts linked to offshore thunderstorms have a peak frequency early in the morning shortly before sunrise, because offshore thunderstorms have their maximum at this time. These wind gusts are known as downbursts or microbursts (Fujita and Byers 1977). A climatology of these events and an overview on the fundamentals of their formation is given in Wakimoto (2001). Basically, there are two mechanisms acting: either downdrafts are produced from the drag of falling precipitation (strong rain or hail) or they come from latent cooling of a larger air mass aloft due to melting, evaporating or sublimation of precipitation. In both cases, downward winds of several tens of metres per second can be produced. When these downdrafts hit the ground, the flow is diverted into the horizontal and a gust front forms which spreads laterally.

These downdrafts can cause extreme structural damage to turbines as was seen in the severe storm event over the Buffalo Ridge Wind Farm on 1 July 2011. At this southwestern Minnesota site, blades from multiple turbines broke away and a tower buckled in the intense winds (Hawbecker et al. 2017).

2.6.2 Tornadoes

While onshore tornadoes mostly form in the afternoon and the early evening at cold fronts or with large thunderstorms when surface heating is at a maximum, offshore waterspouts are more frequent in the morning and around noon when the instability of the marine boundary layer is strongest due to nearly constant sea surface temperatures (SST) and cooling of the air aloft overnight (Dotzek et al. 2010). However, the seasonal cycle is different. Onshore tornadoes most frequently occur in late spring and summer. Offshore waterspouts peak in late summer and early autumn. In this season, the sea surface temperature of shallow coastal waters is still high, while the first autumnal rushes of cold air from the polar regions can lead to an unstable marine boundary layer favourable for waterspout formation (Dotzek et al. 2010).

Although the characteristics of tornado formation are understood in principle today, the prediction of their actual occurrence remains difficult because a variety of different favourable conditions have to be met simultaneously. In general, following Houze (1993) and Doswell (2001), tornado formation depends largely on the following conditions:

- (potential) instability with dry and cold air masses above a boundary layer capped by a stable layer preventing premature release of the instability;
- a high level of moisture in the boundary layer leading to low cloud bases;
- strong vertical wind shear (in particular for mesocyclonic thunderstorms);
- pre-existing boundary layer vertical vorticity (in particular for non-mesocyclonic convection).

A rough estimation how often a tornado could hit a large wind park is given in Sect. 6.7.

2.7 Air Density

Apart from wind speed, the kinetic energy content of the atmosphere also depends linearly on air density [see Eq. (1.1)]. Near-surface air density, ρ, is a direct function of atmospheric surface pressure, p, and an inverse function of air temperature, T. We have from the state equation for ideal gases:

$$\rho = \frac{p}{RT} \tag{2.13}$$

where $R = 287\ \mathrm{J\ kg^{-1}\ K^{-1}}$ is the universal gas constant. Equation (2.13) is equivalent to the hydrostatic Eq. (2.1) above. Figure 2.2 shows air density for commonly occurring values of surface temperature and surface pressure. The figure illustrates that air density can be quite variable. A cold wintertime high-pressure situation could easily come with a density around 1.4 kg/m^3, while a warm

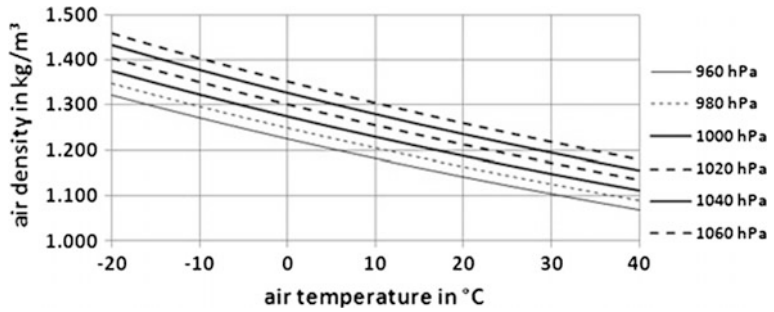

Fig. 2.2 Near-surface air density as function of air temperature and surface pressure

low-pressure situation exhibits an air density of about 1.15 kg/m^3. This is a difference in the order of 20%.

Figure 2.2 is valid for a dry atmosphere. Usually, the atmosphere is not completely dry and the modifying effect of atmospheric humidity has to be considered. Humid air is less dense than completely dry air. Meteorologists have invented the definition of an artificial temperature which is called virtual temperature. The virtual temperature, T_v, is the temperature which a completely dry air mass must have in order to have the same density as the humid air at the actual temperature, T. The virtual temperature is defined as:

$$T_v = T(1 + 0.609q) \tag{2.14}$$

where q is the specific humidity of the air mass given in kg of water vapour per kg of moist air. The temperatures in Eq. (2.14) must be given in K. The difference between the actual and the virtual temperature is small for cold air masses and low specific humidity, but can be several degrees for warm and very humid air masses. Figure 2.2 can be used to estimate air density of humid air masses, if the temperature in Fig. 2.2 is replaced by the virtual temperature. Figure 2.3 gives the increment $T_v - T$ by which the virtual temperature is higher than the actual air temperature as function of temperature and relative humidity of the air for an air pressure of 1013.25 hPa.

Figure 2.3 shows that the virtual temperature increment is always less than 1 K for temperatures below the freezing point, but reaches, e.g. 5 K for saturated humid air at 30 °C. The virtual temperature increment slightly decreases with increasing air pressure. A 1% increase in air pressure (10 hPa) leads to a 1% decrease in the virtual temperature increment. Thus, the determination of the exact density of an air mass requires the measurement of air pressure, air temperature and humidity.

Air density decreases with height, because air pressure decreases with height as given in (2.1). We get from (2.1) or (2.13) (Ackermann and Söder 2000):

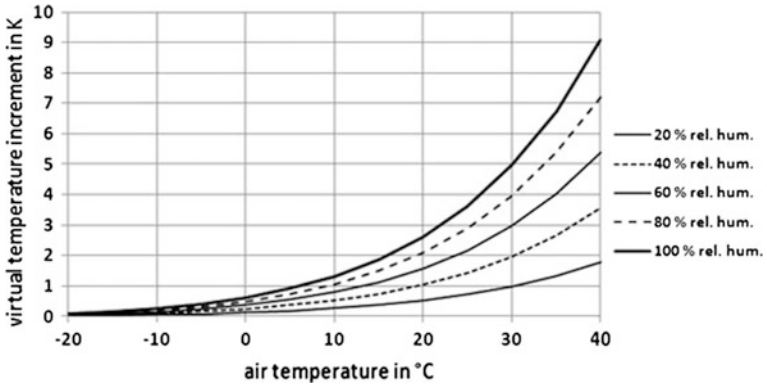

Fig. 2.3 Virtual temperature increment $T_v - T$ in K as function of air temperature and relative humidity for an air pressure of 1013.25 hPa

$$\rho(z) = \frac{p_r}{R\overline{T}} \exp\left(\frac{-g(z - z_r)}{R\overline{T}}\right) \tag{2.15}$$

p_r is the air pressure at a reference level z_r and $\overline{T}$ is the vertical mean temperature of the layer over which the density decrease is computed. Temperature is decreasing with height as well; therefore Eq. (2.15) should only be used for small vertical intervals.

2.8 Thermal Stratification of the Air

We have seen already the effects of temperature on air density in Sect. 2.7 and the influence of large-scale horizontal temperature gradients in Sect. 2.4. Even more important for wind and turbulence conditions is the vertical temperature gradient in the atmosphere. Generally, we distinguish between a neutrally stratified atmosphere, a stably stratified atmosphere, and an unstably stratified atmosphere. An unstably stratified atmosphere is usually observed when cooler air flows over warmer surfaces, while a stably stratified atmosphere forms when warmer air flows over colder surfaces. An unstable atmosphere is connected to an upward turbulent heat flux from the surface into the atmosphere, while a stable atmosphere usually leads to a downward turbulent heat flux from the atmosphere towards the surface.

When analysing atmospheric wind data, it should be recognized that wind speed and atmospheric stability are usually correlated. Unstable conditions are most times found with low wind speeds while stable stratification favours higher wind speeds away from the surface (see, e.g. the Sect. 3.4.2 on low-level jets).Very high wind speeds over rough terrain lead in most cases to turbulent and near-neutral stability conditions.

Vertical motions are enhanced in an unstable atmosphere, while they are oppressed in a stable atmosphere. Therefore, turbulence intensity is higher in an unstable atmosphere than in a neutral atmosphere and smaller in a stable atmosphere. As turbulence leads to vertical mixing, vertical gradients are smaller in an unstable atmosphere and they are larger in a stable atmosphere. Thus, thermal stability of the atmosphere is an important parameter when describing vertical profiles of atmospheric variables, turbulence intensity and other parameters related to these variables. The impact of thermal stratification is largest for small wind speeds and usually gets smaller for higher wind speeds. But the impact of stability also becomes more important for deeper atmospheric layers. Therefore, stability becomes a greater issue for larger wind turbines with higher hub heights.

A neutral atmosphere is characterized by an adiabatic vertical temperature gradient:

$$\frac{\partial T}{\partial z} = -\frac{g}{c_\mathrm{p}} \tag{2.16}$$

where $g = 9.81\ \mathrm{m/s^2}$ is gravity acceleration and $c_\mathrm{p} = 1005\ \mathrm{J/(kg\ K)}$ is the specific heat of the air at constant pressure. This yields a vertical temperature decrease of roughly 1 K per 100 m in an unsaturated atmosphere, i.e. in an atmosphere in which no moisture condensation or evaporation processes take place. Due to this vertical decrease, the normal temperature is not appropriate to identify air masses. For air mass identification, meteorologists and physicists have developed the definition of an artificial temperature which stays constant during vertical displacements without condensation processes. This artificial temperature is the potential temperature, Θ. The potential temperature,

$$\Theta = T\left(\frac{p_0}{p}\right)^{\frac{R}{c_\mathrm{p}}} \tag{2.17}$$

is constant with height in a neutrally stratified air. Here, $R = 287\ \mathrm{J/(kg\ K)}$ is the gas constant for dry air and p_0 is surface pressure. Using this definition, we have stable stratification when $\partial\Theta/\partial z > 0$ and we have unstable stratification when $\partial\Theta/\partial z < 0$. Similar to (2.14), we introduce a virtual potential temperature by including the effect of humidity of the atmospheric stability, because more humid air masses are slightly lighter than dryer air masses:

$$\Theta_v = \Theta(1 + 0.609q) \tag{2.18}$$

Figure 2.4 illustrates atmospheric stability. The full curves indicate absolute temperature, the dashed curves indicate potential temperatures and the dotted lines show the adiabatic temperature change of an air parcel at 500 m which is forced to move upwards or downwards. During stable stratification in the environment (middle frame in Fig. 2.4), an air parcel forced upward is cooler (and therefore heavier) than the environment and thus tries to return to its original position. During

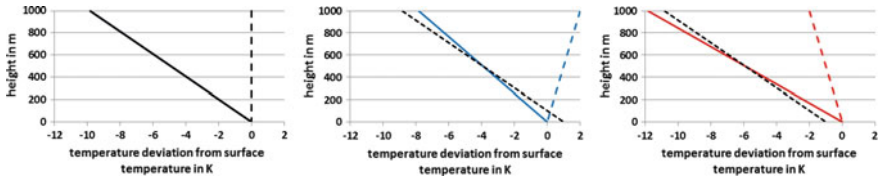

Fig. 2.4 Schematic of vertical temperature profiles (full lines: dry-bulb temperature, long dashes: potential temperature) for neutral stratification (left), stable stratification (middle) and unstable stratification (right). The short-dashed lines in the middle and right frame which have the same inclination as the full curve in the left frame have been plotted so that they intersect the full lines at 500 m above ground

unstable stratification (right frame in Fig. 2.4), an air parcel forced upward is warmer (and therefore lighter) than the environment and thus tries to move further away from its original position. This little consideration shows that stable stratification damps vertical motions, while unstable stratification enhances vertical motions.

For the following considerations in the upcoming chapters, it is advisable to have non-dimensional measures for atmospheric stability. The simplest measure is the 'gradient Richardson number':

$$Ri = \frac{g\frac{\partial \Theta_v}{\partial z}}{\Theta_v\left(\frac{\partial u}{\partial z}\right)^2} \tag{2.19}$$

where u is the wind component in the mean wind direction. Due to the sign of the vertical derivative of the potential temperature, Ri is positive for stable stratification and it is negative for unstable stratification. An even simpler form is the 'bulk Richardson number', Ri_b which is defined as follows:

$$Ri_\mathrm{B} = \frac{g\Delta\Theta_v\Delta z}{\Theta_v(\Delta u)^2} \tag{2.20}$$

where Δz is a chosen height interval and $\Delta\Theta_v$ the vertical potential temperature difference within this height interval. Similar to Ri, Ri_b is positive for stable stratification and negative for unstable stratification. If the bulk Richardson number is used for a layer directly above the surface, it can be simplified to:

$$Ri_\mathrm{B} = \frac{g\Delta\Theta_v z}{\Theta_v u^2} \tag{2.21}$$

The second form of the bulk Richardson number is the most frequently used form in boundary layer studies.

If high-resolution wind fluctuations are known, a 'flux Richardson number', Ri_f can be defined:

$$Ri_{\mathrm{f}} = \frac{g}{\Theta_v \frac{\partial u}{\partial z}} \frac{\overline{w'\Theta'_v}}{\overline{u'w'}} \tag{2.22}$$

where u is the wind component in mean flow direction (and u' the fluctuation of this wind component) and w' is the fluctuation of the vertical wind component (see (7.19) for a definition of this correlation product). Flux Richardson numbers describe the ratio between the turbulent heat flux and the turbulent momentum flux. The heat flux is counted positive if it is directed from the atmosphere towards the ground (cooling the atmosphere) and negative if it is towards the atmosphere (heating the atmosphere). Due to this convention, the flux Richardson number has the same sign as the gradient and the bulk Richardson number.

All three forms of the Richardson number (Ri, Ri_{B}, and Ri_{f}) are different to each other (see Stull (1988) for further details and a discussion of critical values). Thus, the definition of this number must be carefully checked wherever it appears. The ratio between the gradient Richardson number and the flux Richardson number is discussed recently in Grachev et al. (2013).

The square root of the surface value of the turbulent momentum flux, $\sqrt{\overline{u'w'}_0}$ is very often used as a velocity scale in boundary layer meteorology, called friction velocity, u_*:

$$u_* = \sqrt{\overline{u'w'}_0} \tag{2.23}$$

From the surface heat flux, $\overline{w'\Theta'}_0$ and the friction velocity u_* a length scale, L_*, the Obukhov length (sometimes also called Monin–Obukhov length, but the first term is historically more correct and will be used here) can be formed:

$$L_* = \frac{\Theta_v}{\kappa g} \frac{u_*^3}{\overline{\Theta'_v w'}_0} \tag{2.24}$$

where κ is the van Kármán constant which is usually put to 0.4. The ratio z/L_* is used as non-dimensional stability measure in turbulent near-surface air layers (see Chap. 3).

$$\frac{z}{L_*} = \frac{\kappa g z}{\Theta_v} \frac{\overline{\Theta'_v w'_0}}{u_*^3} \tag{2.25}$$

Negative values for z/L_* indicate unstable conditions, while positive values indicate stable conditions. Both z/L_* and all three forms of the Richardson number are zero for neutral conditions. Relations between the second form of the bulk Richardson number (2.21) and the stability parameter (2.25) are given, e.g. in Launiainen (1995) or Grachev and Fairall (1997). The latter give for unstable stratification:

$$\frac{z}{L_*} = CRi_\mathrm{b} \tag{2.26}$$

with C in the order of 10, and for stable stratification:

$$\frac{z}{L_*} = \frac{CRi_\mathrm{b}}{1 - 5Ri_\mathrm{b}} \tag{2.27}$$

Equation (2.27) is said to be valid until z/L* ≈ 0.5. It is not valid for $Ri_\mathrm{b} \geq 0.2$ when the surface layer is no longer fully turbulent.

The virtual potential heat flux $\overline{\Theta_v' w'}$ can be separated into a sensible heat flux and a humidity flux using (2.18):

$$\overline{\Theta_v' w'} = \overline{\Theta' w'} + 0.61\Theta\overline{q' w'} \tag{2.28}$$

The ratio of the turbulent sensible heat flux and humidity flux is called Bowen ratio, B:

$$B = \frac{c_\mathrm{p}\overline{\Theta' w'}}{L_v \overline{q' w'}} \tag{2.29}$$

where q is specific humidity and $L_v \approx 2250$ J/K is the (latent) heat of vaporization. The buoyancy exerted by the vertical heat and humidity gradients is given by $\frac{g}{\Theta}\overline{\Theta' w'} + 0.61 g\overline{q' w'}$. The ratio of these two contributing terms is called the buoyancy ratio, BR which is inversely proportional to the Bowen ratio B:

$$BR = \frac{0.61\Theta\overline{q' w'}}{\overline{\Theta' w'}} = \frac{0.61 c_\mathrm{p}\Theta}{L_v}\frac{1}{B} \tag{2.30}$$

This unstable type of the surface layer is usually found during daytime over surfaces heated by insolation and over waters which are warmer than the air above.

The heat flux allows for the definition of another velocity scale, w_*:

$$w_* = \left(\frac{g z_i}{\Theta}\overline{w'\Theta'}\right)^{1/3} \tag{2.31}$$

This convective velocity scale substitutes the friction velocity as a scaling velocity in situations where vertical velocities due to unstable thermal stratification are in the same order as the horizontal wind speeds.

2.8.1 The Geostrophic Drag Law

Sometimes a stability relation between the surface and the free atmosphere is needed which involve the Coriolis force due to the rotation of the Earth. For this purpose, the non-dimensional stability parameter μ has been introduced:

$$\mu = \kappa \frac{u_*}{fL_*} \tag{2.32}$$

which contains the Coriolis parameter, f. This parameter is identical to the parameter μ_0 introduced in Zilitinkevich (1975).

In cases where high-resolution turbulent fluctuation measurements and wind profile data are unavailable, the large-scale averaged friction velocity can also be inferred from the geostrophic drag law which relates the friction velocity u_* with the modulus, G of the geostrophic wind speed [see Eqs. (2.5) and (2.6)] that represents the large-scale pressure gradient force. The geostrophic drag law reads (Zilitinkevich 1975):

$$C_D = \frac{u_*}{G} = \frac{\kappa}{\sqrt{\left(\ln \frac{u_*}{fz_0} - A\right)^2 + B^2}} = \frac{\kappa}{\sqrt{\left(\ln \frac{G}{fz_0} + \ln C_D - A\right)^2 + B^2}} \tag{2.33}$$

where C_D is the geostrophic drag coefficient, z_0 is the roughness length of the surface introduced in Eq. (3.3).

The friction velocity computed from (2.33) is a large-scale averaged friction velocity, because the geostrophic wind speed is a large-scale feature representing a horizontal scale of the order of about 100 km. The equation was designed in the early times of weather forecast and climate models when an empirical relation between the large-scale geostrophic wind and the overall surface drag force was needed. It is not suited to compute the friction velocity, u_* for small plots.

Unfortunately, Eq. (2.33) is an implicit relation, because the friction velocity appears on both sides of the equal sign. Therefore, simplifications of this drag law have been suggested, e.g. by Jensen (1978). Here, we suggest a similar simplification which has also been used in Emeis and Frandsen (1993). Neglecting B and forming a new parameter $A_* = A - \ln C_D$ gives:

$$\frac{u_*}{G} = \frac{\kappa}{\ln \frac{G}{fz_0} - A^*} \tag{2.34}$$

Equation (2.34) can easily be solved for the friction velocity, if the modulus of the geostrophic wind speed, G, and the parameter A_* are known. Due to the given choice of A_*, the parameter A_* depends on stability (see below) and on surface roughness.

A_*, A and B are empirical parameters which have to be estimated from measurement data. Hess and Garratt (2002) have listed several estimations. They

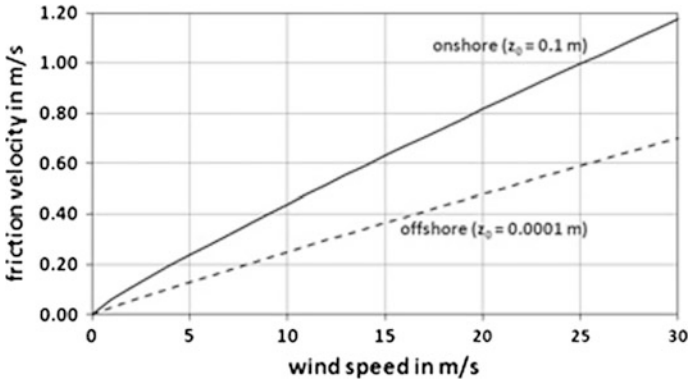

Fig. 2.5 Relation between the geostrophic wind speed, G, and the friction velocity, u_*, using the simplified geostrophic drag law (2.34) with $A_* = 3.8$ for onshore and $A_* = 4.7$ for offshore conditions

suggest, as the best approximation to steady, homogeneous, neutral, barotropic (no thermal wind) atmospheric conditions that they could find, i.e. the near-neutral, near-barotropic ABL in middle and high latitudes, to choose $A = 1.3$ and $B = 4.4$. Using these two values, we get $A_* = 3.7$ for a roughness length of 0.1 m (onshore) and $A_* = 4.5$ for a roughness length of 0.0001 m (offshore). Peña et al. (2010a, b) choose $A = 1.7$ and $B = 5$ to be close to the values used by the wind atlas program WAsP (Troen and Petersen 1989) for neutral conditions. This gives $A_* = 3.8$ for onshore and $A_* = 4.7$ for offshore conditions. The difference between onshore and offshore conditions using the simplified drag law (2.34) is illustrated in Fig. 2.5.

$A = A(\mu)$ and $B = B(\mu)$ depend on the thermal stability μ [defined in (2.32)] of the atmosphere (see Zilitinkevich 1975; Hess and Garratt 2002 or Peña et al. 2010b for details) for non-neutral conditions. Peña and Rathmann (2014) give in consistency with the values used for the European Wind Atlas:

$$A(\mu) = \begin{cases} 1.7 - \sqrt{\mu} & \mu \geq 0 \\ 1.7 + \ln(1 - \mu) & \mu < 0 \end{cases} \tag{2.35}$$

$$B(\mu) = \begin{cases} 5 + \sqrt{\mu} & \mu \geq 0 \\ \frac{5-\kappa}{1-\mu/25} + \kappa & \mu < 0 \end{cases} \tag{2.36}$$

Please note that the parameters G and f are external parameters in the drag law (2.33) and its simplification (2.34). This means, that neither the drag law (2.33) nor its simplification (2.34) can be used to compute a local roughness length-dependent modulus of the geostrophic wind speed. As already stated in Sect. 2.3, the geostrophic wind solely depends on the large-scale horizontal pressure gradient and the latitude-dependent Coriolis parameter, but not on specific small-scale surface properties.

References

Ackermann, T., L. Söder: Wind energy technology and current status: a review. Renew. Sustain. Energy Rev. 4, 315–374 (2000)

Peña, A., O. Rathmann: Atmospheric stability-dependent infinite wind-farm models and the wake-decay coefficient. Wind Energ. 17(8), 1269–1285 (2014)

Doswell, C. A., (Ed.): Severe Convective Storms. Meteor. Monogr. 28(50), 561 pp. (2001)

Dotzek, N., S. Emeis, C. Lefebvre, J. Gerpott: Waterspouts over the North and Baltic Seas: Observations and climatology, prediction and reporting. Meteorol. Z. 19, 115–129 (2010)

Dutton, J. A.: The Ceaseless Wind. Dover Publ., New York, 579 pp. (1986)

Fujita, T. T., Byers, H. R.: Spearhead echo and downburst in the crash of an airliner. Monthly Weather Review, 105, 129–146 (1977)

Grachev; A.A., C.W. Fairall: Dependence of the Monin–Obukhov Stability Parameter on the Bulk Richardson Number over the Ocean. J. Appl. Meteor., 36, 406–414 (1997)

Grachev, A.A:, E.L. Andreas, C.W. Fairall, P.S. Guest, P.O.G. Persson: The Critical Richardson Number and Limits of Applicability of Local Similarity Theory in the Stable Boundary Layer. Bound.-Lay. Meteorol., 147, 51–82 (2013)

Hawbecker, P., Basu, S., Manuel, L.: Realistic simulations of the July 1, 2011 severe wind event over the Buffalo Ridge Wind Farm. Wind Energy, https://doi.org/10.1002/we.2122 (2017)

Hess, G.D., J.R. Garratt: Evaluating models of the neutral, barotropic planetary boundary layer using integral measures. Part I: Overview. Bound.-Lay. Meteor. 104, 333–358 (2002)

Houze, R.A.: Cloud Dynamics. Academic Press, San Diego, 570 pp. (1993)

Jensen, N.O.: Change of Surface Roughness and the Planetary Boundary Layer. Quart. J. Roy. Meteorol. Soc. 104, 351–356 (1978)

Kristensen, L., G. Jensen: Geostrophic Winds in Denmark: a preliminary study. Risø-R-1145(EN), 43 pp. (1999)

Launiainen, J.: Derivation of the Relationship Between the Obukhov Stability Parameter and the Bulk Richardson Number for Flux Profile Studies. Bound.-Lay. Meteorol., 76, 165–179 (1995)

Peña, A., S.-E. Gryning, J. Mann, C.B. Hasager: Length Scales of the Neutral Wind Profile over Homogeneous Terrain. J. Appl. Meteor. Climatol., 49, 792–806 (2010a)

Peña, A., S.-E. Gryning, C. Hasager: Comparing mixing-length models of the diabatic wind profile over homogeneous terrain. Theor. Appl. Climatol., 100, 325–335 (2010b)

Rose, S., P. Jaramillo, M.J. Small, I. Grossmann, J. Apt: Quantifying the hurricane risk to offshore wind turbines. PNAS, published ahead of print February 13, 2012, https://doi.org/10.1073/pnas.1111769109 (2012)

Emeis, S., S. Frandsen: Reduction of horizontal wind speed in a boundary layer with obstacles. Bound.-Layer Meteorol. 64(3), 297–305 (1993)

Stull, R.B.: An Introduction to Boundary Layer Meteorology. Kluwer Acad. Publ., Dordrecht etc., 666 pp. (1988)

Troen, I., E.L. Petersen: European Wind Atlas. Risø National Laboratory, Roskilde, Denmark. 656 pp. (1989)

Wakimoto, R. M.: Convectively driven high wind events. In Severe Convective Storms (pp. 255–298). American Meteorological Society (2001)

Zilitinkevich, S.S.: Resistance laws and prediction equations for the depth of the planetary boundary layer. J. Atmos. Sci., 32, 741–752 (1975)